

Pole Placement Control for Doubly-Fed Induction Generators Using Compact Representations in Complex Variables

Hana Jannaty Baesmat, *Student Member, IEEE*, Marc Bodson, *Fellow, IEEE*

Abstract— The paper presents three algorithms to synthesize a dynamic controller for a Doubly-Fed Induction Generator (DFIG). In each case, the pole placement approach is used to compute the parameters of a feedback controller that regulates the active and reactive powers produced using the rotor voltages. Due to the special structure of the DFIG's model, the analysis and design of the feedback control loop are simplified by transforming its representation into an equivalent system with complex coefficients and half the number of states. This approach yields analytic solutions of the problem with remarkable simplicity. The complex framework facilitates the direct placement of the DFIG system poles in the left half-plane, which ensures stability and performance of the closed-loop system. Additionally, this framework can be used to evaluate the robustness properties of the closed-loop systems. The ability of the synthesized controllers to provide a desirable dynamic and steady-state response is investigated through experiments on a laboratory testbed.

Index Terms— Active and reactive powers, complex domain, doubly-fed induction generators (DFIG), DQ control, full-order pole placement controller, reduced-order pole placement controller, root-locus design.

I. INTRODUCTION

It is estimated that, by 2030, wind power generation may reach 300 GW, which represents 20% of the total energy production [1]. Wind generation units use fixed speed and variable speed turbines [2], but variable speed generators are essential to capture the most power despite varying wind conditions. Amongst the variable speed generators, doubly-fed induction generators (DFIG) with rotor side power electronic converters are very common.

A DFIG generates currents at a fixed frequency on the stator windings whereas the rotor is driven at variable speed [3]. Fig. 1 illustrates a DFIG with its stator windings directly connected to the grid and its rotor windings connected via a back-to-back AC/DC/AC converter. This configuration represents a valuable solution for applications where the range of speed variation is limited. The rating of the AC/DC/AC converter is roughly proportional to the slip and, by limiting the normalized slip to a range of $\pm 30\%$, considerable cost savings can be achieved compared to a system that uses fully-rated power electronics.

Several control techniques have been proposed for the doubly-fed induction machine in the literature among which vector control [2], [4]-[5], also known as Field-Oriented Control (FOC), direct torque [6]-[8] and direct power control [9]-[13] are the most widely-used.

A comparative study of the above techniques was performed in [14]. It was concluded that vector control strategies yielded the lowest THD levels as well as lower instrumentation constraints, whereas direct control methods were up to four times faster than vector control techniques.

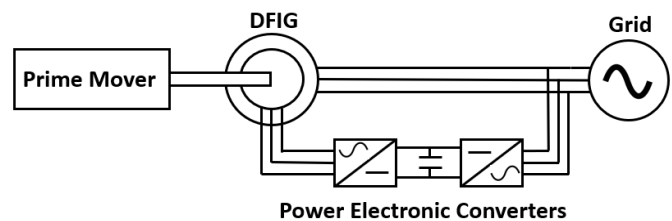


Fig. 1. Schematic diagram of a DFIG

The stability of the DFIG was investigated analytically by Heller *et al.* [15] and Congwei *et al.* [16]. They found that, for certain operating conditions, the system exhibited an unstable behavior, and that the dynamics have poorly-damped eigenvalues with a corresponding natural frequency near the line frequency.

In [17], a coordinated control approach was presented for a reduced-order DFIG that only captured the dynamics of the system that were of significance to the synthesis of the regulator. A state-feedback controller was proposed to control the machine speed, DC bus voltage, and active and reactive powers.

A flatness-based control strategy was proposed in [18] to develop a two-level control structure that decouples the DFIG system into two linear systems. The first level derives the reference values and the second level tracks the reference trajectories. Algebraic equations are then derived to compute the trajectories directly and to control the system's active and reactive powers.

A rotor current control approach was presented in [19] to regulate the active and reactive powers of the DFIG. The proposed controller was designed based on the Optimal

The authors are with the Electrical and Computer Engineering Department, University of Utah, Salt Lake City, UT 84112, USA (e-mail: hana.baesmat@utah.edu; bodson@eng.utah.edu).

Preview Control-LQR (OPC-LQR) method with stator voltage-orientation. Two current control loops were proposed, the slow control loop was designed to control the active and reactive powers of the DFIG and the inner current control loop was designed to compensate for the cross-coupling-induced emf and for the emf due to the stator flux.

In [20], a coordinated control approach between the power electronic converters of the DFIG was proposed to improve the generator's fault-ride-through capability. Nevertheless, the performance of the DFIG under fault conditions falls outside of the scope of this paper.

In this paper, it is shown that an equivalent state-space model with complex states and parameters, and with half the number of states of the original model, simplifies the analysis and design of stator voltage-oriented control laws. In [21], the theory for complex models, which had been used to model AC machines in steady-state, was developed in the frequency and Laplace domains for dynamic analysis. In [22], applications were explored where the analysis of electric machines could be pursued in ways that were not possible in the real domain. The complex Hurwitz test was used in [23] to find parametric conditions for the stability of a stator current controller for a doubly-fed induction machine. It was shown that global stability for a feedback linearized DFIG could be ensured through a proportional-integral (PI) control law that regulated the stator currents. The PI gains had to satisfy a condition that was derived analytically as a simple inequality and had not been found in earlier work in the real domain.

This paper extends the work of [23] by considering a broader class of control laws based on pole placement in the complex domain. Primarily, we demonstrate how the technique facilitates the design of pole placement controllers with relatively simple analytic formulas stating the values of the controller parameters. The pole-placement controllers presented in this paper are of increasing levels of complexity. The first controller uses a steady-state model, the second controller a reduced-order model, and the third controller a full-order model. It is shown through experiments that each of these controllers performs satisfactorily, but more complex controllers exhibit greater ranges of operation and faster convergence.

The novelty of this paper lies in the following:

1. By taking advantage of the special structure of the DFIG, a simplification is made possible. The presented model has half the number of equations, states, and poles (including controller poles) of the original model. The resulting system is analyzed as a single-input single-output complex system, even though the physical system has three inputs and three outputs.

3. By obtaining complex transfer functions from the complex system equations, analytic formulas are obtained for the gains of the control laws that result in a direct placement of the poles at specified locations.

4. All three controllers are analyzed using a complex root-locus method to visualize how the poles of the feedback system move in the stable operating region.

5. The control laws do not use inner current feedback loops requiring separate tuning. Rotor current feedback either is not

needed or is integrated into a control law that exploits the known dynamics of the system. In all cases, tuning can be achieved by adjusting a single parameter specifying the convergence time of the closed-loop system response.

6. The representation in the complex domain yields estimates of robustness similar to the conventional gain and phase margins of single-input single-output systems with real parameters.

II. COMPLEX DOMAIN ANALYSIS

In this paper, we consider systems that can be transformed into systems of smaller dimension but with complex coefficients. The application of design methods in the complex domain relies on a symmetry condition on the system that allows the reduction of the order of the system by 2 and is outlined below [24].

Consider the standard state-space model:

$$\dot{x} = Ax + Bu, y = Cx \quad (1)$$

where the state, input, and output vectors can be split into two vectors of equal dimensions such that:

$$x = \begin{pmatrix} x_1(t) \\ x_2(t) \end{pmatrix}, u = \begin{pmatrix} u_1(t) \\ u_2(t) \end{pmatrix}, y = \begin{pmatrix} y_1(t) \\ y_2(t) \end{pmatrix} \quad (2)$$

whereas

$$A = \begin{pmatrix} A_{11} & -A_{21} \\ A_{21} & A_{11} \end{pmatrix}, B = \begin{pmatrix} B_{11} & -B_{21} \\ B_{21} & B_{11} \end{pmatrix} \\ C = \begin{pmatrix} C_{11} & -C_{21} \\ C_{21} & C_{11} \end{pmatrix} \quad (3)$$

This condition allows the system to be studied through an equivalent complex system with half the dimension by defining complex vectors

$$x_c = x_1 + jx_2, u_c = u_1 + ju_2, y_c = y_1 + jy_2 \quad (4)$$

It follows that

$$\dot{x}_c = A_c x_c + B_c u_c, y_c = C_c x_c \quad (5)$$

where

$$A_c = A_{11} + jA_{21}, B_c = B_{11} + jB_{21}, C_c = C_{11} + jC_{21} \quad (6)$$

It is shown in [21] that any root of $\det(sI - A_c) = 0$ is a root of $\det(sI - A) = 0$. Conversely, if s_0 is a root of $\det(sI - A) = 0$, then either s_0 or its complex conjugate s_0^* is a root of $\det(sI - A_c) = 0$. This implies that, as a result of the unique structure of the state-space model, the roots of $\det(sI - A) = 0$ must either occur in complex pairs or in double real pairs (it is not possible to have single real roots). Then, knowledge of the eigenvalues of A_c provides exact knowledge of the eigenvalues of A : the complete set of poles of the real system can be obtained from the poles of the

complex system [25]. An advantage of the complex domain analysis is that some problems can be solved analytically, as opposed to the real domain analysis where only numerical results can be found. In addition, the complex analysis is often significantly simpler, especially when the complex input and output are scalar. For example, the root-locus of the complex DFIG system has half the branches of the root-locus for the real system and follows rules similar to the root-locus for real systems, with small differences [24]. Also, formulas involving controller gains in vector form reduce to half the number of equations with half the number of variables.

III. COMPLEX MODEL OF THE DFIG IN DQ COORDINATES

The dynamic model of a grid-connected DFIG in dq coordinates (synchronous with the grid) is represented by the following equations.

$$L_s \frac{di_{ds}}{dt} + M \frac{di_{dr}}{dt} = v_{ds} - R_s i_{ds} + \omega_g (L_s i_{qs} + M i_{qr}) \quad (7)$$

$$L_s \frac{di_{qs}}{dt} + M \frac{di_{qr}}{dt} = v_{qs} - R_s i_{qs} - \omega_g (L_s i_{ds} + M i_{dr}) \quad (8)$$

$$L_r \frac{di_{dr}}{dt} + M \frac{di_{ds}}{dt} = v_{dr} - R_r i_{dr} + \omega_s (L_r i_{qr} + M i_{qs}) \quad (9)$$

$$L_r \frac{di_{qr}}{dt} + M \frac{di_{qs}}{dt} = v_{qr} - R_r i_{qr} - \omega_s (L_r i_{dr} + M i_{ds}) \quad (10)$$

where the variables are:

ω_g : grid frequency

ω : mechanical speed

n_p : number of pole pairs

$\omega_s = (\omega_g - n_p \omega)$ is the slip frequency

$i_{ds}, i_{qs}, i_{dr}, i_{qr}$: direct and quadrature components of the stator and rotor currents, respectively

$v_{ds}, v_{qs}, v_{dr}, v_{qr}$: direct and quadrature components of the stator and rotor voltages, respectively

L_s and L_r : stator and rotor inductances, respectively

M : magnetizing inductance

R_s and R_r : stator and rotor resistances, respectively

The state-space model of the DFIG system presented above is available in [8]. To ensure the format of section II, the state and input vectors are re-arranged as follows:

$$x = \begin{bmatrix} i_{ds} \\ i_{dr} \\ i_{qs} \\ i_{qr} \end{bmatrix}, u = \begin{bmatrix} v_{ds} \\ v_{dr} \\ v_{qs} \\ v_{qr} \end{bmatrix} \quad (11)$$

Then, the complex state-space model is written as (1) to (3) by defining:

$$A_{11} = \frac{1}{\sigma L_s L_r} \begin{bmatrix} -L_r R_s & M R_r \\ M R_s & -L_s R_r \end{bmatrix}, B_{11} = \frac{1}{\sigma L_s L_r} \begin{bmatrix} L_r & -M \\ -M & L_s \end{bmatrix}$$

$$A_{21} = \frac{1}{\sigma L_s L_r} \begin{bmatrix} M^2 \omega_s - L_s L_r \omega_g & -L_r M (\omega_g - \omega_s) \\ -M L_s (\omega_s - \omega_g) & -L_s L_r \omega_s + M^2 \omega_g \end{bmatrix}$$

$$B_{21} = \begin{bmatrix} 0 & 0 \\ 0 & 0 \end{bmatrix}$$

$$x_1 = \begin{bmatrix} i_{ds} \\ i_{dr} \end{bmatrix}, x_2 = \begin{bmatrix} i_{qs} \\ i_{qr} \end{bmatrix}, x_c = \begin{bmatrix} i_{ds} + j i_{qs} \\ i_{dr} + j i_{qr} \end{bmatrix}$$

$$u_1 = \begin{bmatrix} v_{ds} \\ v_{dr} \end{bmatrix}, u_2 = \begin{bmatrix} v_{qs} \\ v_{qr} \end{bmatrix}, u_c = \begin{bmatrix} v_{ds} + j v_{qs} \\ v_{dr} + j v_{qr} \end{bmatrix}$$

$$A_c = \frac{1}{\sigma L_s L_r} \begin{bmatrix} \alpha_{11} & \alpha_{12} \\ \alpha_{21} & \alpha_{22} \end{bmatrix}$$

$$B_c = \begin{bmatrix} L_r & -M \\ -M & L_s \end{bmatrix} \quad (12)$$

where

$$\alpha_{11} = -L_r R_s + j(M^2 \omega_s - L_s L_r \omega_g)$$

$$\alpha_{12} = M(R_r - j L_r (\omega_g - \omega_s))$$

$$\alpha_{21} = M(R_s - j L_s (\omega_s - \omega_g))$$

$$\alpha_{22} = -L_s R_r + j(M^2 \omega_g - L_s L_r \omega_s)$$

$$\sigma = \frac{L_s L_r - M^2}{L_s L_r}$$

Note that the system has the desired structure in the state-space, so that the theory can be applied. However, simpler formulas are obtained if one returns to the implicit form (with the inductances on the left-hand side).

By defining complex variables $i_r = i_{dr} + j i_{qr}$, $i_s = i_{ds} + j i_{qs}$, $v_r = v_{dr} + j v_{qr}$, and $v_s = v_{ds} + j v_{qs}$, and applying the Laplace transform, (7) to (10) reduce to:

$$s L_s i_s + s M i_r = v_s - R_s i_s - j \omega_g (L_s i_s + M i_r) \quad (13)$$

$$s L_r i_r + s M i_s = v_r - R_r i_r - j \omega_s (L_r i_r + M i_s) \quad (14)$$

In this paper, the direct axis is assumed to be aligned with the grid voltage vector. Thus, $v_{ds} = v_g$ and $v_{qs} = 0$. Then, the active and reactive powers generated by the DFIG are given by:

$$P_{GEN} = -(v_{ds} i_{ds} + v_{qs} i_{qs}) = -v_g i_{ds} \quad (15)$$

$$Q_{GEN} = -(v_{qs} i_{ds} - v_{ds} i_{qs}) = v_g i_{qs} \quad (16)$$

The negative signs in these equations are due to the direction of the currents assumed in the model. The active and reactive powers can be regulated through the complex stator current i_s , with a desired value i_{sREF} given by:

$$i_{sREF} = \frac{-(P_{REF} - j Q_{REF})}{v_g} \quad (17)$$

where P_{REF} and Q_{REF} are desired values of active and reactive powers, respectively.

IV. TEST BENCH

We discuss the elements of the test bench at this stage, as some of the numerical values are used in the design. The lab test bench includes the following components: Motorsolver DFIG generator and DC motor, dSPACE I/O box connected to dSPACE 1104 board in a PC host, Hirel Power Electronics Drive Board (PEDB), Grid Connection Box, Current Sensor Board.

The Power Electronics Drive Board (PEDB) is an inverter board designed to power the electric machines through two, 3-leg inverters under the control of the dSPACE board. The grid connection box is used to connect the generator windings to the three-phase grid through a relay and a three-phase transformer. The DC motor is used to drive the DFIG. The lab setup for these experiments is shown in Fig. 2.

The parameters for the DFIG are shown in Table I. These parameters are assumed in the design of the controllers in the next sections. To estimate the machine parameters, three-phase voltages were applied to the stator windings at standstill with the rotor open. The stator voltages and currents, and the induced rotor voltages, were measured. From the data, estimates of R_s , L_s , and M were deduced. Then, the roles of the stator and rotor were reversed, resulting in estimates of R_r , L_r , and M . The two estimates of M were close to each other and were averaged to produce a single estimate.

TABLE I
DFIG PARAMETERS

R_s	0.96 Ω	L_s	0.0131 H
R_r	1.04 Ω	L_r	0.0098 H
M	0.0097 H	n_p	2

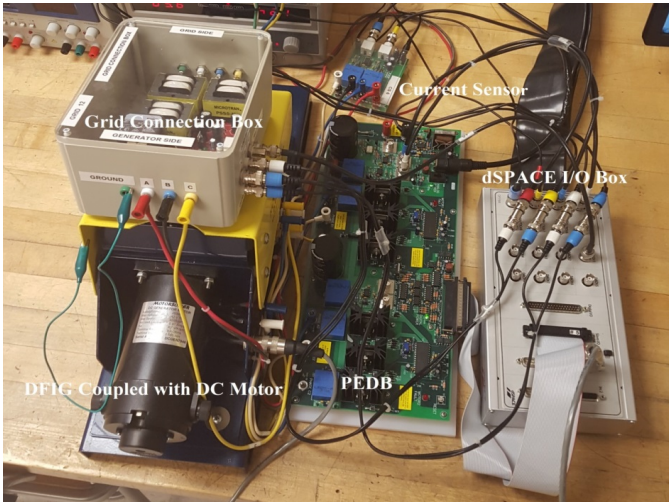


Fig. 2. Test Bench

V. COMPLEX TRANSFER FUNCTION AND CONTROL SYSTEM

The transfer function of the system can be obtained in the complex domain from the complex system equations. The complex open-loop transfer function from v_r to i_s obtained from (13) and (14) is given by:

$$\frac{i_s}{v_r} = \frac{N_o(s)}{D_o(s)} \quad (18)$$

where $N_o(s) = -M(s + j\omega_g)$ and $D_o(s) = \sigma L_s L_r s^2 + (L_s R_r + L_r R_s + j\omega_s \sigma L_s L_r + j\sigma L_s L_r \omega_g)s + (j\omega_g L_s R_r + j\omega_s L_r R_s + R_s R_r - \sigma L_s L_r \omega_g \omega_s)$

Assuming that $n_p \omega = \omega_g$ and using the DFIG machine parameters in section IV, one finds that the open-loop transfer function has one zero at $-j377$ and two poles at $-158.9 - j260.2$

and $-1237.8 - j116.8$. The actual, real domain, open-loop transfer function has 4 poles located at $-158.9 - j260.2$, $-158.9 + j260.2$, $-1237.8 - j116.8$, $-1237.8 + j116.8$. The transfer function also has two zeros at $-j377$ and $+j377$.

Given a complex transfer function for the system, control laws can also be designed for the DFIG in the complex domain. This approach assumes that the controller is subjected to meeting the same symmetry requirements as the DFIG model. The results of the paper show that the control objectives can be achieved within this assumption.

The three-phase to dq transformation is standard in the literature but becomes quite simple using complex variables. Specifically, the complex grid voltage is computed using

$$v_g = \sqrt{2/3} (v_{ag} + v_{bg} e^{j2\pi/3} + v_{cg} e^{-j2\pi/3}) e^{-j\theta_g} \quad (19)$$

where v_{ag} , v_{bg} , and v_{cg} are the three-phase grid voltages and θ_g is an angle chosen such that v_g is real (for grid voltage alignment), i.e.,

$$\theta_g = \angle (v_{ag} + v_{bg} e^{j2\pi/3} + v_{cg} e^{-j2\pi/3}) \quad (20)$$

The complex variables defining the stator and rotor currents are similarly obtained using

$$i_s = \sqrt{2/3} (i_{as} + i_{bs} e^{j2\pi/3} + i_{cs} e^{-j2\pi/3}) e^{-j\theta_g} \quad (21)$$

$$i_r = \sqrt{2/3} (i_{ar} + i_{br} e^{j2\pi/3} + i_{cr} e^{-j2\pi/3}) e^{-j\theta_s} \quad (22)$$

where

i_{as} , i_{bs} , and i_{cs} are the three-phase stator currents
 i_{ar} , i_{br} , and i_{cr} are the three-phase rotor currents
 θ is the mechanical angle

$\theta_s = \theta_g - n_p \theta$ is the angle associated with the slip

From these variables and from the reference values, the control laws discussed in the next section compute the complex rotor voltage v_r . The physical rotor voltages v_{ar} , v_{br} , and v_{cr} are obtained using

$$v_{ar} = \sqrt{2/3} \operatorname{Re}(v_r e^{j\theta_s}), \quad v_{br} = \sqrt{2/3} \operatorname{Re}(v_r e^{j(\theta_s - j2\pi/3)}), \\ v_{cr} = \sqrt{2/3} \operatorname{Re}(v_r e^{j(\theta_s + j2\pi/3)}) \quad (23)$$

Fig. 3 shows the block diagram of the overall DFIG control system. The ‘‘Reference’’ block uses (17) to calculate the reference stator current in the complex domain (i_{sREF}). The ‘‘Grid angle & Mag.’’ block takes the measured three-phase grid voltages (v_{gabc}) and, using (19) and (20) calculates the grid magnitude and angle used by other blocks for transformation from the three-phase to complex variables and vice-versa. The ‘‘abc to complex’’ block, uses equation (21) to convert the

measured three-phase stator currents (i_{sabc}) to the complex domain (i_s). The “xyz to complex” block, uses equation (22) to convert the measured three-phase rotor currents (i_{rxyz}) to the complex domain (i_r). For this conversion, the grid angle (θ_g) as well as the mechanical angle (θ) are utilized.

The “Controller” block generates the rotor voltages (v_r), applied to the DFIG and regulates the generated active and reactive powers. It should be noted that, depending on the controller selected, either the stator currents or the stator and rotor currents as well as the mechanical speed (ω), are utilized to generate the rotor voltages. The detailed design of the controllers is presented in section VI.

v_r is converted from complex to three-phase in the “complex to xyz” block and applied to the Rotor Side Converter (“RSC” block), through PWM modulation (“PWM” block). This conversion is formulated in equation (23). The CS and VS blocks represent the current and voltage sensors for measuring the three-phase stator currents, rotor currents, and grid voltages. The number “3” denotes a three-phase signal.

The simulation model corresponding to Fig. 3 is available on-line [26]. The “Prime mover” block contains the model of a DC motor and the mechanical model for the whole system. Simulation results were reported in [27], whereas this paper reports on experiments. The experiments used the same control code, but the prime mover, DFIG, sensors, actuators, and interfaces were replaced by the physical components. Simulation and experimental results are compared for the third controller in section VI.

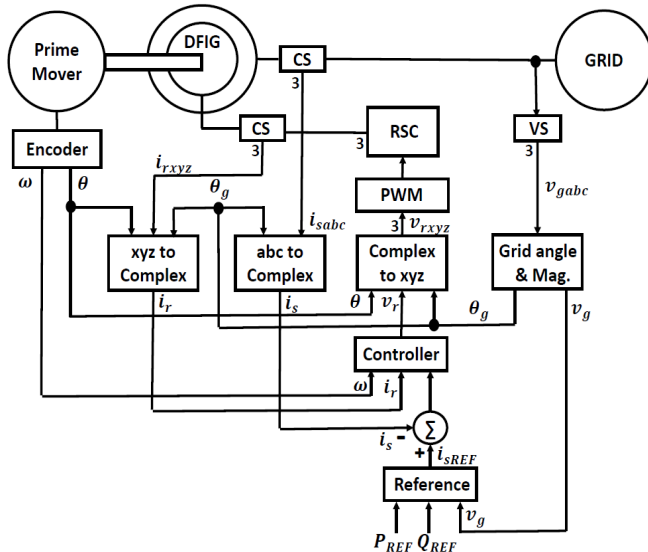


Fig.3. Block diagram of the DFIG control system

VI. COMPLEX CONTROL LAWS FOR THE STATOR CURRENT

A. Integral Controller

One of the simplest control laws that may be conceived for the grid-connected DFIG is the integral control law:

$$v_r = \frac{K_I}{s} (i_s - i_{sREF}) + \frac{R_r}{j\omega_g M} v_g \quad (24)$$

This control law is based on the fact that, using (13) and (14), the complex stator current in steady-state ($s = 0$) and assuming that $n_p \omega \approx \omega_g$, $R_s \approx 0$, satisfies:

$$i_s = \frac{-M}{L_s R_r} v_r + \frac{v_s}{j\omega_g L_s} \quad (25)$$

Under these assumptions, the closed-loop stator current response becomes:

$$i_s = \frac{MK_I}{L_s R_r s + MK_I} i_{sREF} \quad (26)$$

Equation (26) is a first-order system with its pole located at $s = \frac{-M}{L_s R_r} K_I$. This pole can be placed at some desired value a_d in the left half-plane by letting

$$K_I = -\frac{L_s R_r a_d}{M} \quad (27)$$

Equation (24) is represented in the complex domain. However, it can be translated into two equations in the real domain given by:

$$\begin{aligned} v_{rd} &= \frac{K_I}{s} (i_{sd} - i_{sREFd}) + \frac{R_r}{\omega_g M} v_{sq} \\ v_{rq} &= \frac{K_I}{s} (i_{sq} - i_{sREFq}) - \frac{R_r}{\omega_g M} v_{sd} \end{aligned} \quad (28)$$

Note that the imaginary gain in front of the stator voltage results in a coupling of the dq variables, whereas a real gain in front of the stator currents results in propagation along the same axes. Although the complex representation yields a single-input single-output system, the underlying system is a 2x2 multivariable system.

The integral controller was tested on the experimental testbed. The desired pole was set at $a_d = -100$ rad/s. This value corresponds to a 10 ms time constant and 40 ms for a 2% convergence time. 40 ms is equivalent to 2.4 cycles at 60 Hz, which is a reasonable target. For the algorithms of this paper, however, a useful feature is that the controller can be parameterized as a function of the convergence time, which can be set at the user's discretion.

The desired values for the active and reactive powers generated by the DFIG were set at 30 W and 20 VAR, respectively. The result of the experiment for a mechanical speed of $\frac{\omega_g}{n_p}$ RPM, which is the synchronous speed, is shown in

Fig. 4.

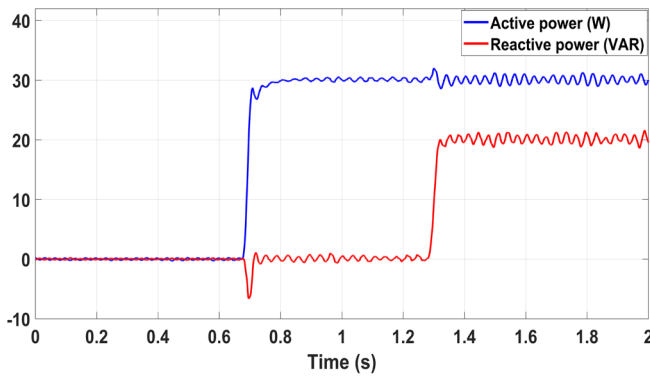


Fig. 4. Simple integral controller

As shown in Fig. 4, the controller reaches the desired values of active and reactive powers. The full-order model DFIG system including the controller has three poles. However, the design of the integral controller is based on a reduced-order system in steady-state and only moves the pole at the origin, without knowledge in the design of the other two stable poles. The root-locus of the first-order system would only show a pole that is moved from 0 to -100. Fig. 5 shows the locus of the three actual DFIG system poles with the integral controller and a gain varying from 0 to nominal corresponding to $a_d = -100$. On the figure, \times and $+$ correspond to the open-loop poles and closed-loop poles for nominal gains, respectively.

As can be seen from this figure, the controller moves the pole at the origin to a value close to -100 (but not exactly, because the extra dynamics of the system were ignored for the design). The other two poles move slightly and remain in the left half-plane.

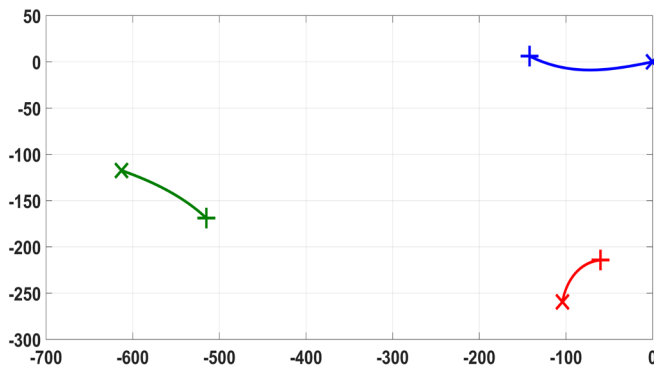


Fig. 5. Root-locus of the third order DFIG model with the simple integral controller

It was verified through experiments that fluctuations in the response tend to dampen with absolute values of a_d smaller than 250 in magnitude and that, for absolute values of a_d greater than about 250, the system becomes unstable. In this case, the pole on the right/bottom of Fig. 5 moves to the right half-plane. The absolute value of a_d should be chosen small enough that the system remains stable, yet large enough that the pole at the origin moves well into the left half-plane, ensuring a fast closed-loop response.

The effect of variable speed operation on the performance of DFIG is discussed next. The mechanical speed is varied from

-30% to +30% from the synchronous speed by applying different steps of voltage to the DC motor. The generated active and reactive powers as well as the percent slip plots obtained from experiments are shown in Fig. 6. The corresponding root-locus diagram of the closed-loop system under variable speed operation is illustrated in Fig. 7.

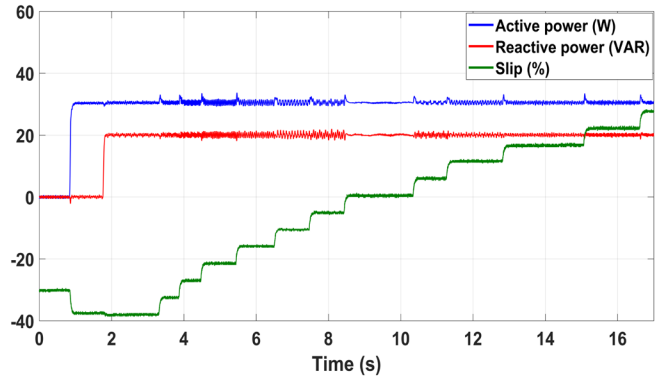


Fig.6. Integral controller with mechanical speed varying from -30% to +30% from synchronous speed, $a_d = -100$

From Fig. 6, it can be concluded that the system remains stable during variable speed operation with minor transients on sudden changes of speed. The root-locus of Fig. 7 corroborates that, when increasing speed from $\frac{0.7\omega_g}{n_p}$ to $\frac{1.3\omega_g}{n_p}$, the system remains in the stable region.

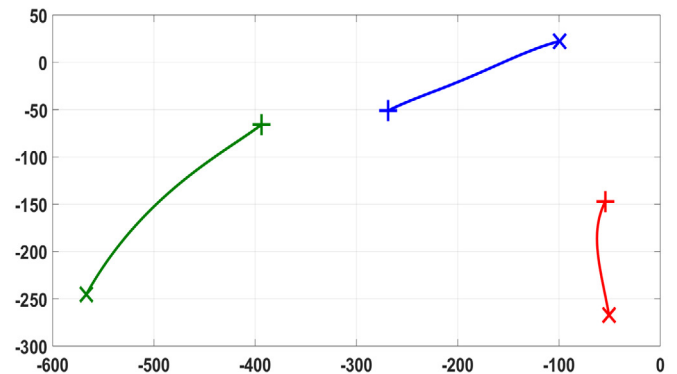


Fig.7. Root-locus of the closed-loop system with the rotor speed varying between -30% to +30% from synchronous speed, $a_d = -100$

Fig. 6 also exhibit oscillations in steady-state with a frequency that varies with the speed of the motor. The frequency content of the oscillations is primarily at twice the slip frequency of the motor and is believed to be due to imperfections in the rotor construction. These effects would be smaller in a large generator, as opposed to the small machine used for the lab experiments.

B. Pole placement controller with a second-order model

Section A introduced an integral control law designed based on the DFIG's steady-state response. In this section, a control law is presented that better accounts for the dynamics of the DFIG by using a reduced-order model. The motivation is that one pole of the DFIG system is much further in the left half-plane when σ is small. To approximate the dominant pole, the

reduced-order model assumes that $\sigma \approx 0$. The previous assumption of $n_p \omega \approx \omega_g$ still holds, but the assumption $R_s \approx 0$ is now removed. A PI controller with complex coefficients is designed so that the complex rotor voltage is described by

$$v_r = K_p(K_F i_{sREF} - i_s) + \frac{K_I}{s}(i_{sREF} - i_s) \quad (29)$$

where K_F is a feedforward gain with a value set at 1/3. A feedforward gain makes it possible to move the zero of the closed-loop transfer function without affecting the closed-loop poles. With a value less than 1, the zero is moved towards the left half-plane.

By plugging in (29) in (14) and noting that $n_p \omega \approx \omega_g$ we have:

$$sL_r i_r + sM i_s = K_p(K_F i_{sREF} - i_s) + \frac{K_I}{s}(i_{sREF} - i_s) - R_r i_r \quad (30)$$

From (13) and (30), the equations of the system can be written as:

$$\begin{pmatrix} sL_s + R_s + j\omega_g L_s & M(s + j\omega_g) \\ s^2 M + K_p s + K_I & s^2 L_r + R_r s \end{pmatrix} \begin{pmatrix} i_s \\ i_r \end{pmatrix} = \begin{pmatrix} v_s \\ (K_p K_{FS} + K_I) i_{sREF} \end{pmatrix} \quad (31)$$

The determinant of the system is:

$$\det \begin{pmatrix} sL_s + R_s + j\omega_g L_s & M(s + j\omega_g) \\ s^2 M + K_p s + K_I & s^2 L_r + R_r s \end{pmatrix} = \sigma L_r L_s s^3 + (L_s R_r + R_s L_r + j\omega_g \sigma L_r L_s - MK_p) s^2 + (R_r R_s - MK_I + j\omega_g L_s R_r - j\omega_g MK_p) s - j\omega_g MK_I \quad (32)$$

which, for $\sigma = 0$, reduces to:

$$(L_s R_r + R_s L_r - MK_p) s^2 + (R_r R_s - MK_I + j\omega_g L_s R_r - j\omega_g MK_p) s - j\omega_g MK_I \quad (33)$$

The denominator of the open-loop transfer function of the second-order model (one DFIG pole and one controller pole) is given by:

$$D_o(s) = \gamma(s - a_0)s \quad (34)$$

where $a_0 = \frac{-(R_r R_s + j\omega_g L_s R_r)}{\gamma}$ and $\gamma = L_s R_r + L_r R_s$.

a_0 approximates the dominant pole of the DFIG and is one of two open-loop poles of the feedback system (the other pole is the controller pole at zero). The proposed design method consists in leaving the pole a_0 at its location whereas moving the pole at the origin to some desired location a_d . This can be achieved by letting K_p and K_I be equal to:

$$K_p = \frac{-(R_r R_s \omega_g - (a_0 + a_d) \gamma \omega_g + j L_s R_r \omega_g^2 - j a_0 a_d \gamma)}{M(\omega_g(a_0 + a_d) - j \omega_g^2 + j a_0 a_d)} \quad (35)$$

$$K_I = \frac{a_0 a_d (\gamma - MK_p)}{-j \omega_g M} \quad (36)$$

Then, the transfer function of the closed-loop system from i_s to i_{sREF} becomes:

$$i_s = \frac{N_c(s)}{D_c(s)} i_{sREF} \quad (37)$$

where

$$\begin{aligned} D_c(s) &= (\gamma - MK_p)(s - a_0)(s - a_d) \\ N_c(s) &= -K_F K_p M \left(s + \frac{K_I}{K_p K_F} \right) (s + j\omega_g). \end{aligned} \quad (38)$$

The locus for the closed-loop poles assuming the reduced-order model is shown in Fig. 8 for $a_d = -100$ and $\omega = \frac{\omega_g}{n_p}$.

The experimental results of the active and reactive powers generated by the DFIG are shown for $a_d = -100$ and $\omega = \frac{\omega_g}{n_p}$ on the top of Fig. 9. The root-locus assuming the full order model is shown on the bottom of the figure and is different from the root-locus of Fig. 8, due to the extra pole. However, the root-locus of Fig. 8 is a reasonable approximation for the movement of the dominant poles.

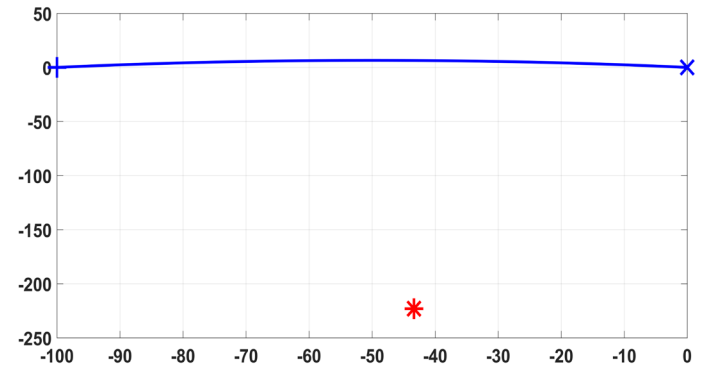
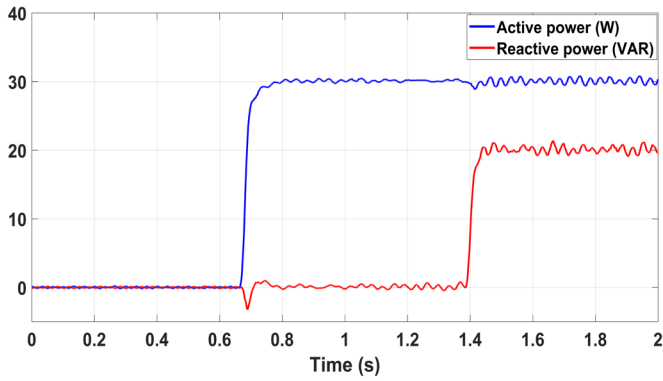
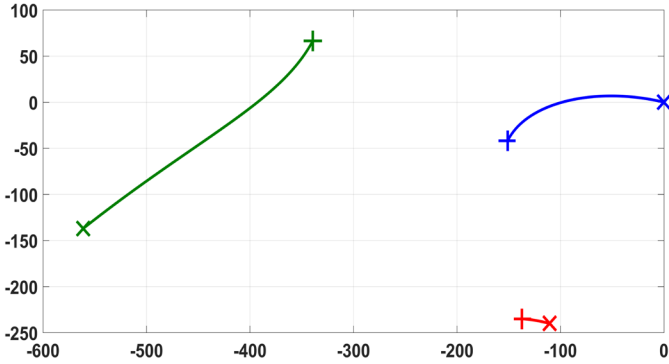


Fig.8. Root-locus of the second-order DFIG model with the controller also based on a second-order model

This control law yields a stable system for values of a_d up to 400 in magnitude. A wider range is obtained than for the first integral controller, resulting in a faster response. This is due to controlling the DFIG dominant pole as well as the controller pole. The controller also performs well during operation across a wide range of speeds, as shown in Fig. 10. Fig. 11 shows the movement of the poles with the speed variation. All poles remain in the left half-plane as the speed increases from $\frac{0.7\omega_g}{n_p}$ to $\frac{1.3\omega_g}{n_p}$.



(a)



(b)

Fig. 9. (a) Generated powers by the DFIG (b) Root-locus of the third-order DFIG model with the controller based on a second-order model

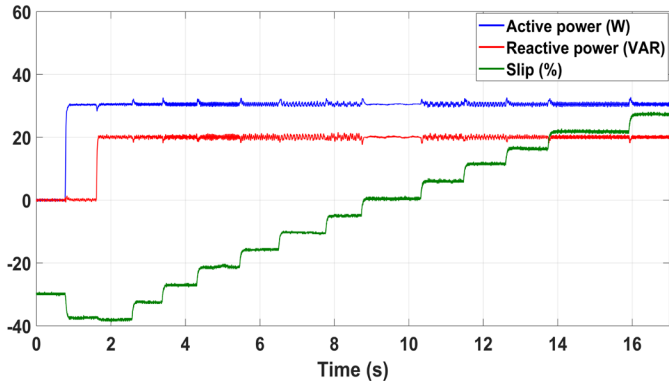


Fig. 10. Second-order controller with mechanical speed varying from -30% to +30% from synchronous speed, $a_d = -100$

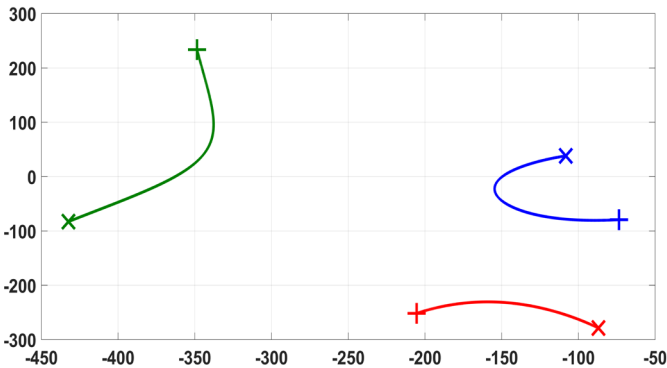


Fig. 11. Root-locus of the closed-loop system with the rotor speed varying between -30% to +30% from synchronous speed, $a_d = -100$

C. Pole placement controller with a third-order model

The third control law is designed to place all three poles of the DFIG system with a control law:

$$v_r = R_r i_r + j\omega_s (L_r i_r + M i_s) + K_p (K_F i_{sREF} - i_s) + \frac{K_I}{s} (i_{sREF} - i_s) - K_R i_R \quad (39)$$

This control law contains a term that neutralizes the speed-dependent terms in the right-hand side of (14), as well as feedback terms from both the stator and the rotor currents, allowing one to place all three poles of the system. The feedback terms in (39) make the system a linear time-invariant system. The remainder of the control law is then a state-feedback controller with constant feedback gains. The states of the system include the states of the DFIG and the state of the integrator that was added to ensure perfect tracking of constant references.

Unlike the first two control laws, this controller does not assume that $n_p \omega \approx \omega_g$, $\sigma \approx 0$, or $R_s \approx 0$, and takes into account the full dynamics of the model. K_p , K_I , and K_R are determined by pole placement techniques for the third-order model.

For this purpose, by plugging in (39) in (14), we have:

$$sL_r i_r + sM i_s = K_p (K_F i_{sREF} - i_s) + \frac{K_I}{s} (i_{sREF} - i_s) - K_R i_r \quad (40)$$

(14) and (40) can be rewritten as:

$$\begin{pmatrix} sL_s + R_s + j\omega_g L_s & sM + j\omega_g M \\ s^2 M + K_p s + K_I & s^2 L_r + K_R s \end{pmatrix} \begin{pmatrix} i_s \\ i_r \end{pmatrix} = \begin{pmatrix} v_s \\ (K_p K_F s + K_I) i_{sREF} \end{pmatrix} \quad (41)$$

Then

$$W = \det \begin{pmatrix} sL_s + R_s + j\omega_g L_s & sM + j\omega_g M \\ s^2 M + K_p s + K_I & s^2 L_r + K_R s \end{pmatrix} = \sigma L_r L_s s^3 + (L_s K_R + R_s L_r + j\omega_g \sigma L_r L_s - M K_p) s^2 + (R_s K_R + j\omega_g L_s K_R - M K_I - j\omega_g M K_p) s - j\omega_g M K_I = \sigma L_r L_s (s^3 + A_1 s^2 + A_2 s + A_3) \quad (42)$$

gives the poles of the system.

By specifying desired values of the poles through the variables A_1, A_2, A_3 , it is possible to solve (42) for K_p, K_I , and K_R and place all the poles at the specified locations. Specifically, let the desired values of the poles be a_{d1}, a_{d2} , and a_{d3} . The equation to be solved is

$$W = \sigma L_r L_s ((s - a_{d1})(s - a_{d2})(s - a_{d3})) \quad (43)$$

so that, with

$$A_1 = -(a_{d2} + a_{d1} + a_{d3}), A_2 = (a_{d2} a_{d1} + a_{d2} a_{d3} +$$

$$a_{d3}a_{d1}), A_3 = -a_{d2}a_{d3}a_{d1} \quad (44)$$

The control gains are then found to be given by

$$K_I = \frac{j\sigma L_r L_s A_3}{M\omega_g} \quad (45)$$

$$K_P = \frac{1}{MR_s} \left((R_s + j\omega_g L_s)(L_r R_s - A_1 \sigma L_r L_s + jL_r L_s \sigma \omega_g) + L_s \left((A_2 \sigma L_r L_s) + \frac{1}{\omega_g} (jA_3 \sigma L_r L_s) \right) \right) \quad (46)$$

$$K_R = \frac{1}{R_s} \left(A_2 \sigma L_r L_s + \frac{1}{\omega_g} (jA_3 \sigma L_r L_s) + (j\omega_g (L_r R_s - A_1 \sigma L_r L_s + jL_r L_s \sigma \omega_g)) \right) \quad (47)$$

One possibility would be to place all the poles at the same location. However, as was confirmed by experiments, it is counterproductive to move open-loop poles that are far in the left half-plane. Therefore, desired poles were specified in consideration of the open-loop poles. The root-locus and experimental vs. simulation results for $a_{d1} = -100$, $a_{d2} = -130.5 - j240$, $a_{d3} = -521.2 - j137.1$, and $\omega = \frac{\omega_g}{n_p}$, are shown in Fig. 13. These values correspond to moving the pole at origin to -100 and slightly moving the other two poles of the system in the left half-plane. The value of K_F was set at 1/100. The top of Fig. 13 shows that the simulation is a close representation of the real system; however, as mentioned earlier, oscillations in the response obtained from experiment are not present in simulation and are likely due to the machine imperfections. Simulation results for the other two controllers were presented in [27].

The effect of operation away from the synchronous speed on the performance of the controller is shown in Fig. 14. As can be seen from Fig. 14, this controller performs very well under variable speed operation with almost no transients on steps of mechanical speed. The superior transient response of this controller is due to the location of all the poles remaining unchanged with varying mechanical speeds. It was found that the value of a_{d1} could be increased in magnitude all the way to 1000 in magnitude.

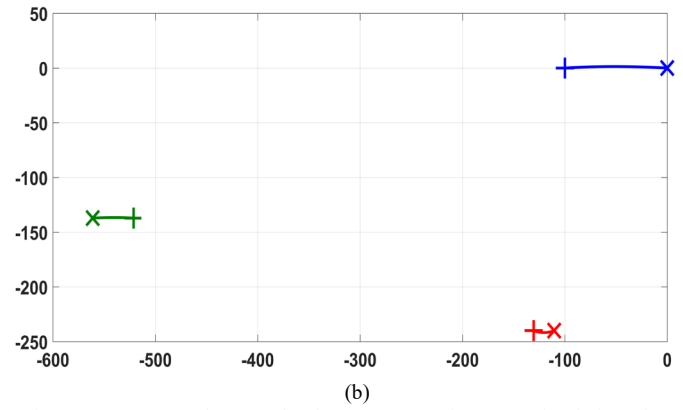
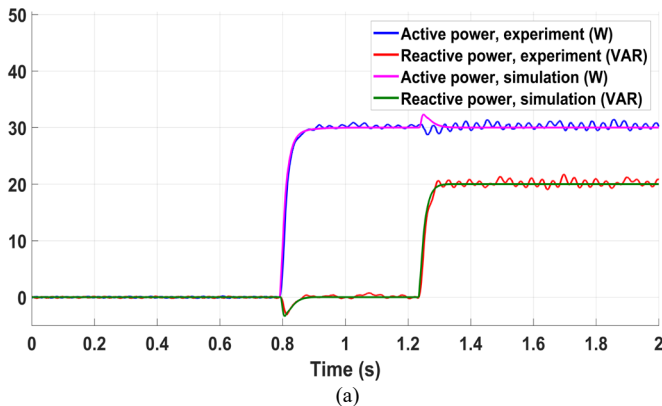


Fig. 13. (a) Generated powers by the DFIG (experiment vs. simulation) (b) Root-locus of the third-order DFIG model with the controller also based on a third-order model

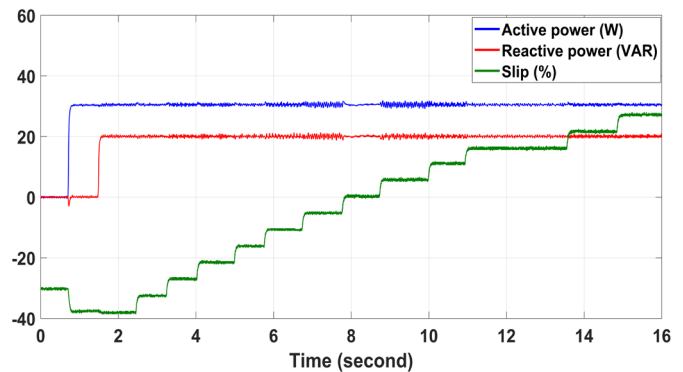


Fig. 14. Third-order controller with mechanical speed varying from -30% to +30% from synchronous speed, $a_d = -100$

VII. ROBUSTNESS ANALYSIS

The robustness of the closed-loop systems can be evaluated by expressing the overall system as a 2x2 feedback system with real parameters. However, some information can be gathered from the complex system representation as well. Gain margins, phase margins, and time delay margins can be computed to quantify the robustness to changes of gain, phase, and delay in the rotor voltages [21].

Fig. 15 shows the Nyquist plots corresponding to controller #1 for $a_d = -100$ and $a_d = -250$. Note that the curves for positive frequency (labelled PF) and negative frequency (labelled NF) are not symmetric as for real transfer functions. For $a_d = -100$, the diagram gives a gain margin of 7.3dB and a phase margin of 52 deg (determined by the negative frequency curve). For $a_d = -250$, the NF curve reaches the critical point and the system is at the edge of instability, as was observed earlier.

Fig. 16 gives the curve of controller #2 for $a_d = -1000$ and $a_d = -400$. For $a_d = -100$, the diagram gives a gain margin of 21.7dB and a phase margin of 59.4 deg (this time determined by the positive frequency curve). For $a_d = -400$, the PF curve reaches the critical point and the system is at the edge of instability. This is also consistent with previous observations.

Fig. 17 gives the curves of controller #3 for $a_d = -100$ and $a_d = -1000$. For $a_d = -100$, the diagram gives an infinite gain margin and a phase margin of 89.5 deg. For $a_d = -1000$,

the system is still stable.

A more complete assessment of robustness would require a quantitative representation of unmodeled dynamics. However, the Nyquist curve of the complex system rapidly gives an estimate of robustness similar to the conventional gain and phase margins of single-input single-output systems with real parameters.

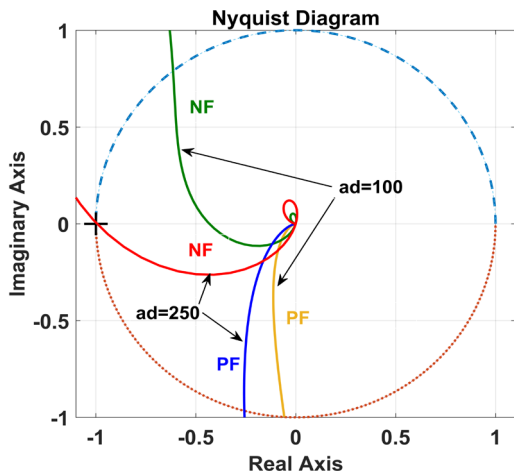


Fig. 15. Nyquist diagram of controller #1 for $a_d = -100$ and $a_d = -250$

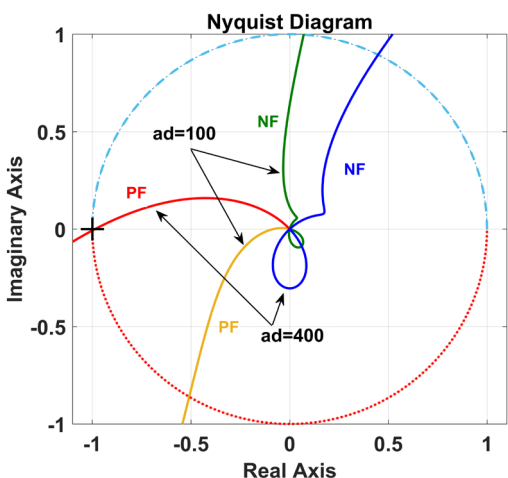


Fig. 16. Nyquist diagram of controller #2 for $a_d = -100$ and $a_d = -400$

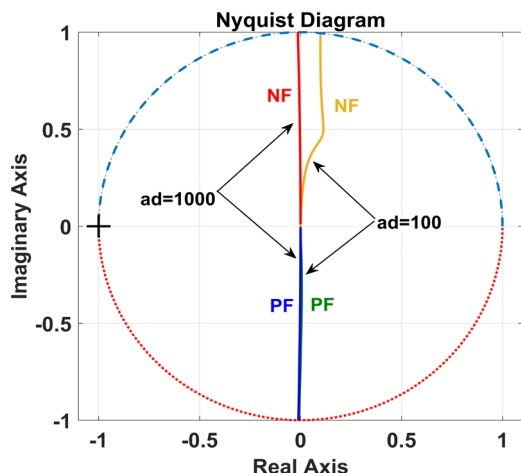


Fig. 17. Nyquist diagram of controller #3 for $a_d = -100$ and $a_d = -1000$

VIII. COMPARISON OF THE CONTROLLERS

All three controllers moved the controller pole at the origin to -100 in the left half-plane. Depending on the design of the controllers, greater values in magnitude were possible and other poles of the system either were not considered or were moved slightly in the left half-plane. Even the simplest controller worked well in tracking references of active and reactive powers. Aside from its simplicity, an advantage is that it does not require sensors for the rotor currents. The second controller, based on a reduced-order model, only requires sensors for the stator currents, as the first controller, and is only slightly more complex. This controller demonstrates a superior response under variable speed operation and exhibits a faster response time with smaller amplitude of fluctuations and overshoot compared to the first controller. The third controller places all three poles of the full-order complex model at desirable locations in the left half-plane. Rotor current measurements are used to achieve this result with a state-feedback controller. In contrast with the first two controllers, the third controller uses speed data to ensure consistent performance across the speed range. The resulting controller proved to be stable for all operational speeds and provided the best transient responses.

The three controllers demonstrate the power of the complex system representation. The system with three rotor inputs and three stator outputs becomes a much simpler single-input single-output system. Equations that would have been represented using 2-D vectors in conventional dq control become simple scalar equations. Root-locus analysis can be applied that involves half the number of branches. Compact analytic expressions define the controller gains that are needed to place the poles at desired locations. In particular, it would be relatively simple to update in real-time the controller parameters based on estimates of the machine parameters. To some extent, testing and debugging of the control algorithm is also simplified with the complex representation.

IX. COMPARISON WITH PREVIOUS METHODS

The method presented in this paper can be viewed as an extension of the algorithm found in [23]. However, the controllers presented in this paper directly place the system poles in the left half-plane, ensuring stability and performance of the closed-loop system. This makes the design and implementation processes as well as the stability analysis simpler. Other control schemes presented in the literature do not investigate the stability of the overall system [18]-[20], or present robustness measures.

Compared to other methods found in the literature [20], [28], the proposed schemes are different in that they do not rely on inner loops to regulate the rotor currents. Note that it is not possible to control the stator and rotor currents separately using the rotor voltages. Therefore, the algorithms of this paper are designed to directly regulate the stator currents, with reference values obtained from the active and reactive power references. Constraints on the references may be applied to ensure that rotor currents do not exceed their limits. The full-order pole

placement controller proposed in the paper uses the known dynamics to combine the rotor current measurements with the stator current measurements in a stable system. Tuning of the feedback system is achieved through direct and intuitive adjustments of the desired pole locations.

The control laws were evaluated on a laboratory testbed, as opposed to the simulations that are often used for such systems [18]-[19], [27]-[28]. As valuable as simulations are, various effects appear in experiments that are not modelled in simulations and significantly affect the performance. The validation provided by the experiments of the paper give a valuable confirmation that the methods proposed are potential candidates for larger generators.

X. CONCLUSIONS

The paper proposed to design control laws for doubly-fed induction generators using a compact system representation in the complex domain. The simplification of the representation enabled the derivation of analytic formulas for pole placement. Three controllers of increasing complexity were proposed. The first controller was designed based on the steady-state model of the DFIG and used a simple integral controller to control the stator currents through the rotor voltages. The second controller used a reduced-order model that took into account the dynamics of the DFIG but ignored a remote pole of the system. Finally, the last controller placed all three complex poles of the third-order DFIG model with integral action at desired locations. The effectiveness of the proposed controllers was evaluated in experiments. The three controllers were shown to perform well with appropriate design choices. The main contribution of the paper, however, was not to claim superiority of any controller over another, but to show that control design could be achieved with greater simplicity in the complex domain, that compact formulas for pole placement could be derived with this approach, and that effective feedback control could be achieved in practice with this approach.

XI. REFERENCES

[1] S. Lindenberg, B. Smith, and K. O'Dell, "20% wind energy by 2030," DOE, Golden, CO, US, Rep. DOE/GO-102008-2567, July 2008.
[2] S. Muller, *et al.* "Doubly fed induction generator systems for wind turbines," *IEEE Ind. Appl. Mag.*, vol. 8, no. 3, pp. 26-33, May/June 2002.
[3] N. Bianchi, L. Alberti and S. Bolognani, "A design-oriented model of doubly-fed induction machine," *IEEE International Electric Machines and Drives Conference (IEMDC)*, Niagara Falls, 2011, pp. 557 – 562.
[4] R. Datta and V. T. Ranganathan, "A simple position-sensorless algorithm for rotor-side field-oriented control of wound-rotor induction machine," *IEEE Trans. Ind. Electron.*, vol. 48, no. 4, pp. 786–793, Aug. 2001.
[5] Q. Li, *et al.*, "Stator current vector control strategy of doubly fed induction generator using proportional-resonant regulators," *The Journal of Engineering*, vol. 2017, issue. 13, pp. 1728-1733, 2017.
[6] G. Abad, J. Lopez, *et al.*, "Direct Control of the Doubly Fed Induction Machine" in *Doubly fed induction machine, modeling and control for wind energy generation*, Piscataway, NJ: John Wiley & Sons, 2011, pp. 244.
[7] G. S. Buja and M. P. Kazmierkowski, "Direct torque control of PWM inverter-fed AC motors—A survey," *IEEE Trans. Ind. Electron.*, vol. 51, no. 4, pp. 744–757, Aug. 2004.
[8] S. Arnalte, *et al.*, "Direct torque control of a doubly-fed induction generator for variable speed wind turbines," *Electr. Power Compon. Syst.*, vol. 30, no. 2, pp. 199–216, 2002.

[9] R. Datta and V. T. Ranganathan, "Direct power control of grid-connected wound rotor induction machine without rotor position sensors," *IEEE Trans. Power. Electron.*, vol. 16, no. 3, pp. 390–399, May 2001.
[10] L. Xu and P. Cartwright, "Direct active and reactive power control of DFIG for wind energy generation," *IEEE Trans. Energy. Convers.*, vol. 21, no.3, pp. 750–758, Sep. 2006.
[11] P. Zhou, *et al.*, "Improved direct power control of a DFIG-based wind turbine during network unbalance," *IEEE Trans. on Power Electronics*, vol. 24, no. 11, pp. 2465-2474, 2009.
[12] J. Hu, *et al.*, "Predictive Direct Virtual Torque and Power Control of Doubly Fed Induction Generators for Fast and Smooth Grid Synchronization and Flexible Power Regulation," *IEEE Trans. Power Electron.*, vol. 28, no. 7, pp. 3182 – 3194, 2013.
[13] J. Hu, *et al.*, "Predictive Direct Power Control of Doubly Fed Induction Generators Under Unbalanced Grid Voltage Conditions for Power Quality Improvement," *IEEE Trans. Sustain. Energy*, vol. 6, issue. 3, pp. 943-950, 2015.
[14] E. Tremblay, *at al.*, "Comparative Study of Control Strategies for the Doubly Fed Induction Generator in Wind Energy Conversion Systems: A DSP-Based Implementation Approach," *IEEE Trans. Sustain. Energy*, vol. 2, issue. 3, pp. 288-299, 2011.
[15] M. Heller and W. Schumacher, "Stability analysis of doubly-fed induction machines in stator flux reference frame," *Proc. EPE '97 Conf.*, vol. 2, Brussels, Belgium, Sep. 8–10, 1997, pp. 707–710.
[16] L. Congwei, *et al.*, "Research of stability of double fed induction motor vector control system," in *Proc. ICEMS'01 Conf.*, vol. 2, Shenyang, China, Aug. 18–20, 2001, pp. 1203–1206.
[17] M. Bejaoui, *et al.* "Control of doubly-fed induction generator for wind energy in network context," *IET Renew. Power Gen.*, vol. 8, issue. 2, pp. 109-118, March 2014.
[18] M. H. Variani, *et al.*, "Two-Level Control of Doubly Fed Induction Generator Using Flatness-Based Approach," *IEEE Trans. Power Syst.*, vol. 31, no. 1, pp. 518-525, 2016.
[19] B. Subudhi and P. S. Ogeti, "Optimal preview stator voltage-oriented control of DFIG WECS," *IET Gener. Transm. Dis.*, vol. 12, issue. 4, pp. 1004-1013, 2018.
[20] M. Q. Duong, *et al.*, "A Comparative Study on Controllers for Improving Transient Stability of DFIG Wind Turbines During Large Disturbances," *Energies*, vol. 11, issue. 3, 2018, DOI: 10.3390/en11030480.
[21] L. Harnefors, "Modeling of three-phase dynamic systems using complex transfer functions and transfer matrices," *IEEE Trans. on Industrial Electronics*, vol. 54, no. 4, pp. 2239-2248, 2007.
[22] M. Bodson and O. Kiselychynk, "The complex Hurwitz test for the analysis of spontaneous self-excitation in induction generators," *IEEE Trans. on Automatic Control*, vol. 52, no. 2, pp. 449–454, 2013.
[23] A. Dòria-Cerezo, *et al.*, "Study of the stability of a direct stator current controller for a doubly fed induction machine using the complex Hurwitz test," *IEEE Trans. on Control Systems Technology*, vol. 21, no. 6, pp. 2323-2331, 2013.
[24] A. Dòria-Cerezo and M. Bodson, "Root locus rules for polynomials with complex coefficients," *Proc. of the 21st Mediterranean Conference on Control & Automation (MED)*, Chania, Crete, 2013, pp. 663 – 670.
[25] M. Bodson, "Design of controllers in the complex domain," *Proc. of the 53rd IEEE Conference on Decision and Control*, Los Angeles, CA, 2014, pp. 4077-4082.
[26] www.ece.utah.edu/~bodson/code
[27] H. Baesmat and M. Bodson, "Design of Pole Placement Controllers for Doubly-Fed Induction Generators in the Complex Domain," *Proc. of the 2015 IEEE Power & Energy Society General Meeting (PES)*, Denver, CO, 2015, pp. 1-5.
[28] Y. Liu, *et al.*, "Primary frequency control of DFIG-WTs using bang-bang phase angle controller," *IET Gener. Transm. Dis.*, vol. 12, issue 11, pp. 2670-2678, 2018.